Energy 228 (2021) 120654

Contents lists available at ScienceDirect

Energy

journal homepage: www.elsevier.com/locate/energy

Experimental and modeling investigation of water adsorption of hydrophilic carboxylate-based MOF for indoor moisture control

Kan Zu, Menghao Qin*

Department of Civil Engineering, Technical University of Denmark, Lyngby, 2800, Denmark

ARTICLE INFO

Article history:
Received 18 September 2020
Received in revised form
29 March 2021
Accepted 12 April 2021
Available online 18 April 2021

Keywords:
MOF
Adsorption dynamics
Modelling
Indoor moisture control
Energy conservation

ABSTRACT

Metal-organic frameworks (MOFs) have been considered as one of the most promising candidates for the sorption-based moisture control owing to higher energy efficiency compared to conventional refrigeration-based systems. In this study, MOF-based desiccant (MIL-160) was prepared and studied for water vapor adsorption. MIL-160(Al) consists of Al-based metal clusters and biomass-derived organic link, which is a green and environmentally-friendly material for indoor climate control. Here ad/desorption isotherms were measured and fitted based on the Langmurian sorption theory. These isotherms indicated that MIL-160(Al) was a hydrophilic material with a turning point at 8%P/P0. The sorption performance was also investigated and simulated on a 3-D heat and mass transfer model, which was then validated by a series of tests of the vapor sorption at the metal plate. Considering some simplified postulations (e.g. constant isosteric heat during ad/desorption process, linear driving force theory, equivalent thermal conductivity of materials), the effect of different parameters on the moisture transport were successfully investigated such as the thickness of MOF layer, porosity, and diffusivity, etc. In this regard, the simulated results together with the validation provide important insights into the MIL-160(Al) used desiccant system.

1. Introduction

In the past decades, the total building energy consumption has sharply increased over the world, in which electricity demand for heating, ventilation, and air conditioning (HVAC) systems accounts for more than 40% of total building energy consumption [1,2]. To improve the thermal comfort of the living space, more and more buildings are supplied with HVAC systems to deal with the indoor thermal load. Thus, low energy consumption in air-conditioning systems is crucial to the sustainable development of global energy strategy.

In general, the total cooling load of a building consists of sensible and latent loads. Traditional air conditioners counterbalance both latent and sensible loads by cooling the process air below the dew point and then reheating to the desired air condition. Though the refrigeration dehumidification can achieve the final purpose, the resulted low evaporation temperature (5–7 °C) and reheating process have a great impact on the coefficient of performance (COP) [3]. In addition, the refrigeration process can even cause severe ozone depletion and global warming by taking HCFCs or HFCs as refrigerants [4]. In order to reduce energy consumption, it is essential to develop some other technologies to make an easy-to-operate and environmentally friendly system [5,6]. One promising choice to upgrade such systems is through the introduction of a solid desiccant air-conditioning system based on the adsorption and desorption mechanism [7,8]. Many studies indicated that solid desiccant systems can offer many advantages, as they can not only make use of solar energy and waste heat as an energy source to drive the system but also usually utilize non-toxic and easily available water as the adsorbate. However, one critical problem to limit the widespread application is the low loading lift of conventional desiccants (i.e. silica gel and zeolite) during an adsorption cycle, which means that lower loading lift in per unit kilogram of desiccant material needs more desiccants employed to meet the required sorption loading. This results in the complexity and bulky size of the whole system [9]. In addition, the amount of the cyclic loading lift directly depends on the desiccant [10], whose interaction to adsorbate and intrinsic structure can affect the vapor pressure equilibrium and the operating temperature. In this regard, the selection of desiccants with high adsorption properties can

* Corresponding author.
E-mail address: menqin@byg.dtu.dk (M. Qin).

https://doi.org/10.1016/j.energy.2021.120654
0360-5442/

potentially promote the COP for the air conditioning system [6,11].

Metal-organic framework (MOF) has emerged as an ideal candidate for the application in both closed adsorption heat pump and open desiccant dehumidifiers due to its highly tunable and remarkable porosity properties. It is known that MOFs are mainly constructed by the integration of metal clusters and organic ligands with microporous structure and homogeneous. Many reports have demonstrated that many MOFs have S-shaped water uptake isotherms, high cycling performance, and milder regeneration temperature [12–14]. Seo et al. [15] had demonstrated that two hierarchically porous MOFs, MIL-100, and MIL-101, are workable to dehumidification with high hydrothermal stability and sorption capacity. Xu et al. [16] had compared the dehumidification performance of HKUST-1 with silica gel by experimenting with the full-scale desiccant coated heat exchangers. A numerical study of MIL-101 based cooling system had been carried out by Bareschino et al. [17], which shows higher dehumidification performance than the silica gel-based one. Besides, many studies [18,19] had experimentally investigated the sorption performance of different MOF materials based on the closed water-sorption-driven chillers. The applications in the dehumidification scenario are also expected.

Recently, a green metal-based MOF, MIL-160, has been proposed for the sorption-based solid desiccant system, which featured cost-effective and non-toxic properties. The cycling water loading lift is higher than many traditional and conventional materials (i.e. silica gel, SAPO-33) [13,20–23], and the adsorption performance is sensitive to temperature at low relative pressure. Serre et al. [24] firstly proposed a hydrothermally stable and biomass-derived porous material, named MIL-160(Al), using the solvothermal method. As an isostructural solid to CAU-10, this Al-based MOF shows a more excellent performance in the heat transformation than some commercial materials such as SAPO-34. Later on, a series of tests on the open-system prototype were carried out to exhibit its superior energy-storage capacities and stability, and the optimized and green synthesis method paved the way for large-scale production [25]. Wharmby et al. [26] used Rietveld method to investigate the phase transition of MIL-160(Al) during water adsorption. Cui et al. [27] have conducted a series of experiments to measure the heat properties (i.e. specific heat capacity, thermal conductivity, isosteric heat) of MIL-160(Al), which provides important information to the water adsorption applications.

To date, MIL-160(Al) is reported as a new kind of green and biomass-based MOF material, featured in large-scale production and good sorption performance. However, little literature has reported the applications of MIL-160(Al) in the open solid desiccant systems for indoor moisture control. Herein, we aim to investigate the sorption dynamics of MIL-160(Al) to enhance its operation performance on the material level during the adsorption and desorption processes. Firstly, hydrophilic Carboxylate-based MOF MIL-160(Al) was synthesized through solvothermal methods, and then the characterization and water adsorption were carried out as shown in section 2. To determine the equilibrium equations for the corresponding isotherms, the Langmurian sorption isotherm model was introduced to fit with the measured water adsorption data. A detailed mathematical model based on MOF desiccants was then developed to elucidate the heat and mass transfer mechanisms between desiccants and the surrounding air. The governing equations and methodology of the water-MOF pair were demonstrated in sections 3 and 4, respectively. Except for the material properties, the other required parameters (e.g. isotherms model, isosteric heat, diffusivity, etc.) were obtained from fitting or calculation based on the existed equations, and then the kinetics simulation using MIL-160(Fe) were discussed in section 5 to predict the adsorption dynamics, which is validated by adsorption tests. Finally, the parameter studies (i.e. cycle time, porosity and operation conditions, etc.) were conducted. Under these simple operational principles, the adsorption-based air-conditioning systems can achieve indoor hygrothermal control through water vapor adsorption and desorption.

2. Experiments

2.1. Synthesis

MIL-160(Al) can be synthesized by the solvothermal synthesis route via the chemical reaction of Aluminum acetate and FDCA (2,5-furandicarboxylicacid). 1:1 of Aluminum acetate and FDCA were mixed in a container filled with deionized water, and then stirred for 24 h under the reflux condition. The reaction product was purified by deionized water and ethanol at room temperature for 3 h and finally dried in a vacuum oven (100 °C) to produce the light yellow solid MIL-160(Al) [27].

2.2. Material characterizations

Before isotherms measurements, the morphologies of MIL-160(Al) were characterized using a scanning electron microscope (SEM). Fig. 1 shows the microstructure of the MOF samples, illustrating the intercrystalline voids between pillar-shaped crystals. These connected voids would further widen the area of interface between crystals and vapor, which facilitate vapor diffusion. Table 1 has provided the basic structural information about MIL-160(Al).

2.3. Isotherms and kinetics

A gravimetric analyzer (dynamic vapor sorption, DVS) was utilized to measure the isotherms and kinetics of this carboxylate-based MOFs by taking advantage of its high accuracy and stability in the temperature and humidity control during the whole experiments. There are two holders (reference and sample holders, 5 g ± 0.1 μg each) suspended on each side of the microbalance in the DVS apparatus. Since the microbalance can directly detect the variation of adsorbent mass over time, DVS can record the adsorbent mass as a function of relative pressure and time under a given temperature. The schematic configuration of the DVS is shown in Fig. 2. Inside the DVS, a built-in heater provides the isothermal environment, and the humidifier generates the required amount of water vapor. Dry N_2 (99.999% purity) is ducted to purge the system before the test, and the mass flow controller connected to a control panel can autonomously control the vapor pressure of the mixture (dry and saturated vapor gas) to the set value. The test conditions are measured by the humidity and temperature probes close to the sample holder. Noting that it is required to calibrate the temperature and humidity sensors to reduce the measurement error for each test.

Prior to the tests, the activation process is conducted via vacuum heating at 120 °C for at least 1 h. MIL-160(Al) sample of 50 mg has been loaded on the sample holder. During the measurements of isotherms, the ad/desorption processes at different vapor partial pressure run after the drying process of the test sample. There are 13 test points of vapor partial pressure, and the sample approaches the saturated state in each test point if the ratio of mass variation meets the conditions of <0.03%. In addition, the stepwise pressure increase (Adsorption) or decrease (Desorption) is adopted at each set test point. For isotherms tests, the temperature of the test chamber ranges from 30 to 50 °C, and the vapor pressure from 1Pa to 12000Pa. As for the measurements of kinetics, the gravimetric analyzer was controlled with the temperature in the range from 20 to 45 °C at 65%RH.

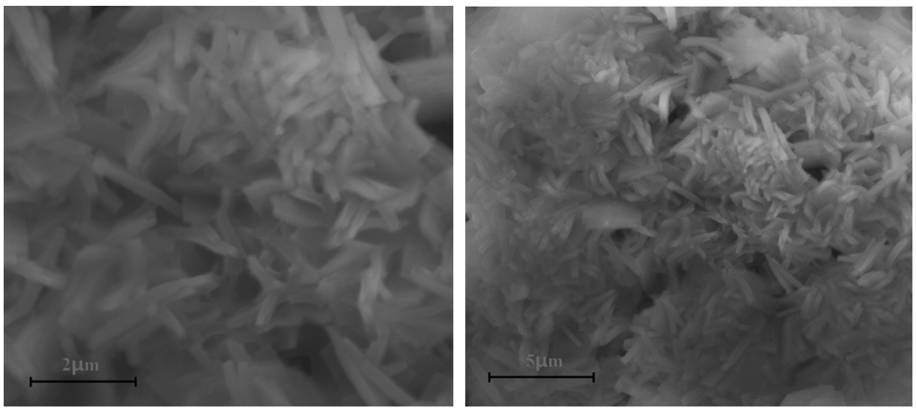

Fig. 1. SEM photos of MIL-160(Al) showing the crystal structure.

Table 1
Porous properties of MIL-160(Al).

	BET surface area ($m^2\ g^{-1}$)	Pore volume ($cm^3\ g^{-1}$)	Pore diameter (nm)
MIL-160(Al)	~1200	0.4	0.5

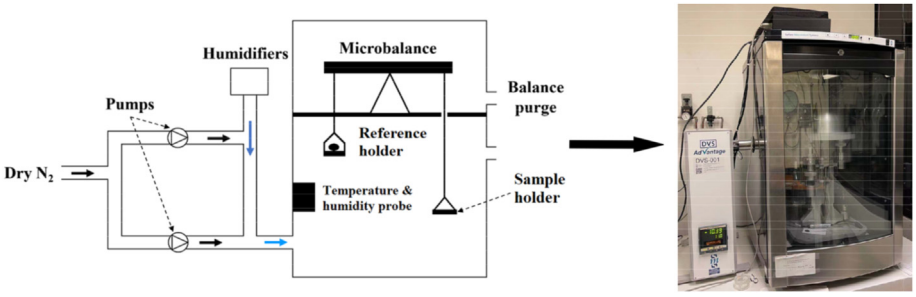

Fig. 2. Schematic illustration of the gravimetric analyzer for the measurement of water uptake.

2.4. Sorption performance

In Fig. 3, the ad/desorption performance tests were conducted on a MOF-coated metal plate, which was put in a climate-controlled small chamber. The temperature and humidity level was controlled by an air conditioner and a humidifier to provide the inlet vapor flux with the given temperature and humidity value. Two pair of temperature and humidity sensors were assembled respectively at the inlet and inside the climate chamber. The bottom side of the metal plate (4 cm × 4 cm × 0.05 cm) was attached to a thermostatic electric heater to control the whole ad/desorption temperature ($T_s = 20\ ^\circ C$ for adsorption; 70 °C for desorption). MOF samples with the thickness of 0.25 mm and 0.8 mm were prepared and coated on the other side of the metal plate. The climate conditions at the chamber were maintained at 21 °C, 65%RH.

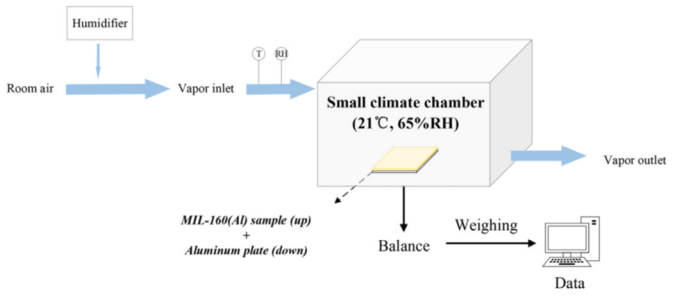

Fig. 3. The setup of sorption performance tests.

3. Mathematical modeling

A transient multi-dimensional mathematical model to describe heat and mass transfer was developed in this section to predict the ad/desorption performance under moist air. To model the sorption behaviors, Fig. 4 shows the schematic of the simulation model for the adsorption dynamics, which consists of moisture transport inside the desiccant and heat transfer in the desiccant and a thin aluminum plate (supporting the MOF block). This model was built based on the experiments in Section 2.3. In order to clearly describe the whole ad/desorption state, a 3D model has been built to show the impact from space geometry, which is a 3D coordinate system with time dependence (x, y, z, t). Besides, considering that many different mechanisms are involved in the adsorption and desorption of porous materials, the overall transport of water inside the desiccant and from the desiccant to the moist air is a complex process. There are some assumptions on the proposed mathematical model:

- There was no dead air zone in the test chamber, and the distribution of temperature and humidity are even in the climate chamber;

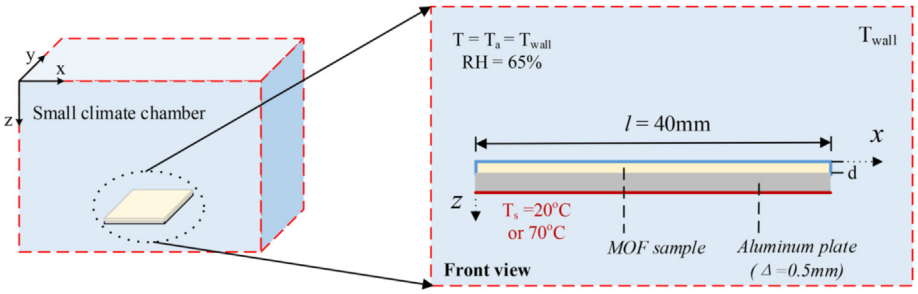

Fig. 4. The schematic of the simulation model.

- The surrounding air states were maintained at the given value;
- The size of the desiccant in the z-direction are uniform;
- The water vapor within the intercrystalline voids is assumed to meet the ideal gas state;
- Crystal size, porosity, and mass distribution are spatially uniform;
- The physical properties are not related to temperature (i.e. thermal conductivity, isosteric heat) but depend on water uptake.

3.1. Moisture transport within MOFs

The mass change of vapor over the desiccant zone can be written by Refs. [28–30]:

$$\frac{\partial \rho}{\partial t} + \nabla \cdot (\rho u) = \nabla \cdot D_v \nabla \rho - \rho_d \frac{1-\varepsilon}{\varepsilon} \frac{\partial \omega}{\partial t} \tag{1}$$

where ρ and are the vapor concentration in the intercrystalline air and the density of desiccant [kg m^{-3}]; ε is the porosity of desiccant; ω is the amount of the adsorbed vapor inside the desiccant crystals [kg kg^{-1}], and $\frac{\partial \omega}{\partial t}$ represents the adsorption rate at a given time and space. According to the Darcy's law and equation of state ($P = \rho R_v T$), the velocity vector of vapor over the porous medium is given by:

$$u = -\frac{A}{\mu} \cdot \nabla P = -\frac{A R_v}{\mu} (\rho \nabla T + T \nabla \rho) \tag{2}$$

$$A = \frac{d^2 \varepsilon^3}{150(1-\varepsilon)^2} \tag{3}$$

As for the intercrystalline vapor diffusion D_v, it can be obtained by the following equation.

$$D_v = \frac{\overline{d}}{3} \sqrt{\frac{8 R_v T}{\pi}} \tag{4}$$

where μ is the dynamic viscosity of vapor [kg $(m \cdot s)^{-1}$]; ∇P is the pressure gradient within the intercrystalline pore; $\overline{d}$ represents the average size of intercrystalline pores that can be calculated as a function of crystal size and overall porosity [m].

3.2. Heat transfer within MOFs

Considering that heat and mass transfer simultaneously occurs throughout the adsorption and desorption process, equivalent heat capacity, heat conduction, and adsorption heat are governed by energy conservation, which can be calculated as [28,29]:

$$\overline{\rho c}\left(\frac{\partial T}{\partial t} + u \nabla \cdot T\right) = \nabla \cdot \lambda_{eq} \nabla T + q_{ah} \rho_d (1-\varepsilon) \frac{\partial \omega}{\partial t} \tag{5}$$

$$\overline{\rho c} = (1-\varepsilon)\rho_d (c_{pm} + \omega c_{pw}) + \varepsilon \rho c_{pv} \tag{6}$$

where q_{ah} represents the isosteric heat during ad/desorption [J kg^{-1}]. It is noted that when the ambient vapor was adsorbed within the desiccant, the thermodynamic property of the vapor phase was similar to its liquid phase, accompanied by the release of adsorption heat. According to the Clausius- Clapeyron equation, the adsorption heat (q_{ah}) can be estimated by

$$q_{ah} = \frac{R \partial ln P}{\partial\left(-\frac{1}{T}\right)} \tag{7}$$

Based on the adsorption model shown in Eq. (9), this equation is a function of adsorption uptake fraction (ω_{eq}). In Eq. (6), it can be found that the average volumetric heat capacity [J $(kg \cdot K)^{-1}$] consists of desiccant, c_{pm}, adsorbed vapor, c_{pw} and the vapor phase, c_{pv}. Here the average thermal conductivity is therefore estimated by employing a modified Zehner-Schlunder model [31]:

$$\lambda_{eq} = \left(1-\sqrt{1-\varepsilon}\right)\lambda_v + \left(1-\sqrt{\varepsilon}\right)\lambda_m + \left(\sqrt{1-\varepsilon} + \sqrt{\varepsilon} - 1\right) * \left[\frac{k\left(1-\frac{\lambda_v}{\lambda_m}\right)}{\left(1-\frac{k^* \lambda_v}{\lambda_m}\right)^2} ln \frac{\lambda_m}{k^* \lambda_v} - \frac{k-1}{1-\frac{k^* \lambda_v}{\lambda_m}}\right], \quad k = \left(\frac{1-\varepsilon}{\varepsilon}\right)^{0.9676} \tag{8}$$

3.3. S-shaped isotherm model

The experimentally measured water uptake has been used to fit with the sorption isotherm model, which theoretically shows the sorption behavior of vapor-MOF pair under different vapor pressure and operating temperature conditions. In order to simplify the above-mentioned governing equations, Langmurian type isotherm has been applied to disclose the relationship of the equilibrium concentration of adsorbed vapor with the vapor pressure, P, and temperature, T. In this case, the S-shaped isotherm model can be written as below [9]:

$$\theta = \frac{\omega_{eq}}{m_0} = \frac{K\left(\frac{P}{Ps}\right)^{\alpha}}{1 + (K-1)\left(\frac{P}{Ps}\right)^{\alpha}} \tag{9}$$

where, θ is the fractional water uptake; ω_{eq} and m_0 are the amount of the adsorbed water vapor [kg kg^{-1}] and limiting uptake [kg kg^{-1}]; α is the factor that can be obtained from adsorption experiments; P_s and P is the saturated vapor pressure and vapor pressure [Pa], respectively. According to Langmuir analogy, the equilibrium constant K here can be expressed as $\beta \exp(\alpha \cdot \Delta Q/RT)$. β is the fitting coefficient; α indicates the heterogeneity factor; ΔQ represents the adsorption characteristics energy.

Considering the calculation of adsorption rate, $\frac{d\omega}{dt}$, a linear driving force model can be applied and simplified [28,32,33]:

$$\frac{d\omega}{dt} = \frac{60}{d^2} D_s(\omega_{eq} - \omega) \tag{10}$$

where D_s indicates the vapor diffusion inside the desiccant crystal [m^2 s^{-1}]. The evaluation of D_s is given and simplified by $D_s = a_1 \cdot \exp(-a_2/RT)$, where a_1 and a_2 can be obtained from experiments [28]. In this way, the average adsorption rate ($\frac{d\omega}{dt}$) can be calculated by plugging Eq. (9) into Eq. (10). Then Eqs. (1) and (5) together with Eq. (10) describe the adsorption dynamic model for moisture transport.

3.4. Initial and boundary conditions of the desiccant-coated humidity pump

The initial conditions for the whole MOF crystals are:

$$T(x,y,z,0) = T_0, \rho(x,y,z,0) = \rho_0, \omega(x,y,z,0) = \omega_{eq}(P_0, T_0) \tag{11}$$

The boundary conditions for the whole MOF crystals are:

$$\begin{aligned}\rho(0,y,z,t) = \rho(L,y,z,t) = \rho(x,0,z,t) = \rho(x,W,z,t) \\ = \rho(x,y,0,t) = \rho(x,y,H,t) = \rho_a\end{aligned} \tag{12}$$

$$T_{plate}(x,y,-H_p,t) = T_s = \begin{cases} T_c, \ Adsorption \\ T_h, \ Desorption \end{cases} \tag{13}$$

$$\frac{\partial \rho}{\partial z}|_{z=0} = 0 \tag{14}$$

$$T(x,y,0,t) = T_{plate}(x,y,0,t) \tag{15}$$

$$n \cdot \lambda_{eq} \nabla T|_{y=H,\ x=0} = h_v(T_a - T) + \varepsilon\sigma\left(T_w^4 - T^4\right) \tag{16}$$

where ε is the emissivity of the sample surface to the environment. Noted that in order to calculate the sorption performance (Fig. 3), Fig. 4 shows that the Dirichlet boundary is set for vapor transfer and the third boundary is prepared for heat transfer. The other parameters mentioned are listed in Table 2.

3.5. Simulation methodology

In the context, the governing equations and auxiliary equations Eqs. (1)–(10) were solved by employing the finite difference scheme for heat and mass transfer in the desiccant and air. The computational operation was conducted on COMSOL using structured meshing for the sorption simulation model shown in Fig. 4. The operation conditions were consistent with the experiments, which is listed in Table 3. It is worth mentioning that variable time steps have been adopted to expedite the calculation while ensuring good convergence. In this regard, the time step of 0.01s was set considering the relatively large differences at the beginning stage of simulations. As the calculation continued, the finite difference of vapor concentration in each node was reduced. Then the time steps in the following calculation were gradually increased up to 0.5s. To avoid any abnormal results, convergences have been achieved by setting tolerance as 1e-6.

4. Results and discussion

In the following section, the evaluation of some parameters such as isosteric heat and intracrystalline diffusivity has been made to do the model calculations, which are compared with the validation experiments. Subsequently, parameter studies have been investigated to observe the effect of different material properties and geometry to the sorption performance of MIL-160(Al).

4.1. Sorption isotherm model

Based on the gravimetric analyzer, the experimentally measured water uptake of MIL-160(Al) was shown in Fig. 5, and the results indicated that the isotherms were almost S-shaped during the adsorption process, which is resulted from the uniform pore size in the material. The fitting curves from the Langmurian sorption isotherm [9] match well with the experimental data. This means that the fitting equation from Eq. (9) can describe the water uptake of MIL-160(Al) under different vapor pressure and temperature on the adsorption dynamic model. These measured isotherms also indicated that MIL-160(Al) is sensitive to temperature variation. Every 10 °C increase in the temperature leads to obvious changes in the turning point (P/P0), at which the material starts the adsorption process. The maximum water uptake at 30 °C can approach ~0.38 g g^{-1}. The fitting parameters were shown in Table 4.

4.2. Isosteric heat of MIL-160(Al)

Since the isotherm model can predict the water uptake with different vapor pressure and the surrounding temperature, the isosteric heat can therefore be calculated through the Clausius–Clapeyron model in Eq. (7). Based on the Langmurian analogy, it is found in Fig. 6 that vapor pressure [ln(P)] against temperature [1/T] varies linearly with different water uptake fractions (θ). In Fig. (6), the slope of ln(P) to 1/T equals $-q_{ah}/R$, thus the calculated isosteric heat was 52–54 kJ mol^{-1}, barely varying against the adsorbed water. Compared with the measured results [27], the relative errors of these values were 4–8%. In the following simulation, we adopted the average value of isosteric heat, which is 53 kJ mol^{-1}.

4.3. Intracrystalline diffusivity

Intracrystalline diffusivity plays an important role in the diffusion of the adsorbed water. In order to describe the variation of the adsorbed water vapor in Eq. (10), this value was obtained through the measurement of sorption kinetic on MIL-160(Al). Based on the Fick's law, the adsorbed vapor mass fraction can be expressed and simplified as follows:

$$\frac{\omega_t}{\omega_\infty} = 1 - \sum_{n=1}^{\infty} \frac{6}{(\pi n)^2} \exp\left(-\frac{(2n\pi)^2 D_\mu}{d^2} t\right) \tag{17}$$

where ω_∞ represents the amount of the adsorbed water vapor as

Table 2
Adsorption properties in the simulation of moisture transport.

Parameter	Symbol	value
MIL-160(Al)		
Density	ρ_d	400–600 kg m^{-3}
Specific heat capacity	c_p	1600 J $(kg \cdot K)^{-1}$
Thermal conductivity	λ_m	0.07 W $(m\ K)^{-1}$
Porosity	ε	0.4
Crystal size	d	1.5×10^{-6}m
Thermal conductivity of water vapor	λ_v	0.018 W $(m\ K)^{-1}$
Thermal conductivity of metal plate	λ_{plate}	2770 W $(m\ K)^{-1}$
Specific heat of water vapor	c_{pv}	$-2 \times 10^{-7}T^3 + 5.9 \times 10^{-4}T^2 + 0.11T + 1790$
Specific heat of adsorbed water vapor	c_{pw}	4200 J $(kg\ K)^{-1}$
Specific heat of metal plate	c_{pm}	960 J $(kg\ K)^{-1}$

Table 3
The operation conditions of experiments.

Operation conditions	Symbol	Value
Initial temperature	T_0	21 °C
Initial vapor concentration	ρ_0	0.0118 kg m^{-3}
Bottom temperature	T_s	20 °C, AD 70 °C, DE

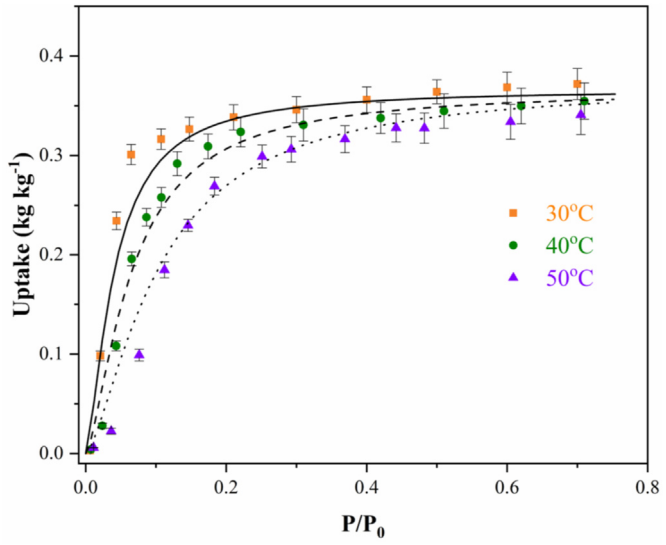

Fig. 5. Sorption isotherms of MIL-160(Al) under different temperature conditions. Here, scatters represent experimental data, curves indicate fitting curves (R-square: 0.9678).

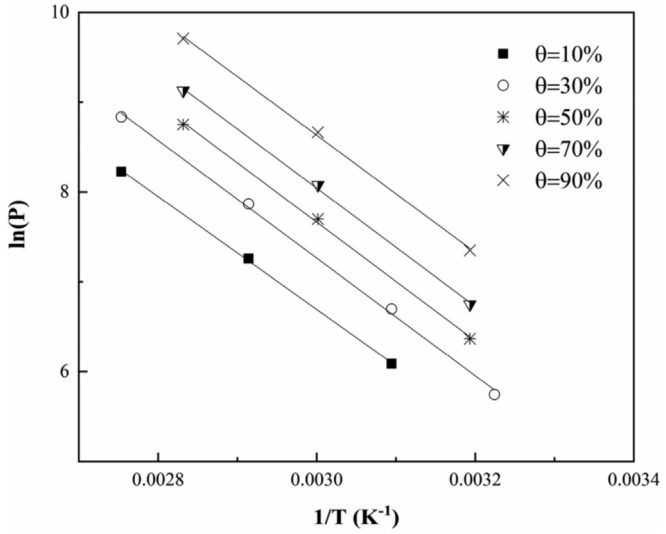

Fig. 6. Isosteric heat of water vapor adsorption on MIL-160(Al) for different water uptake fractions.

$$\ln\left(\frac{D_s}{a_1}\right) = -\frac{a_2}{RT_s} \tag{18}$$

Eq. (18) indicated that there is a linear relationship between intracrystalline diffusion (D_s) and the inverse temperature, which conforms to the measured data shown in Fig. 7. a_1 and a_2 are calculated as 1.05×10^{-11} m^2 s^{-1} and 28299 J mol^{-1}, respectively. Consequently, Eq. (18) can be inserted into Eq. (10) to solve the

Table 4
Fitting information of Langmurian model for MIL-160(Al) – water system.

	m_0	α	ΔQ	β
MIL-160(Al) + water vapor	0.39 kg kg^{-1}	1.192	1469 kJ kg^{-1}	1.1178×10^{-4}

the time approaches to ∞.

From Eq. (17), it can be found that the corresponding intracrystalline diffusion (D_s) can be obtained from the fitting results when given the average crystal size of 1.5 μm. According to the linear driving force model [31], the intracrystalline diffusivity function can be expressed based on Eq. (10) and rewritten as:

mathematical model.

4.4. Sorption simulation

4.4.1. Model validation

As described in the experimental section, the measurements of sorption performance were conducted with two different bottom side surface temperatures 20 °C (Adsorption) and 70 °C

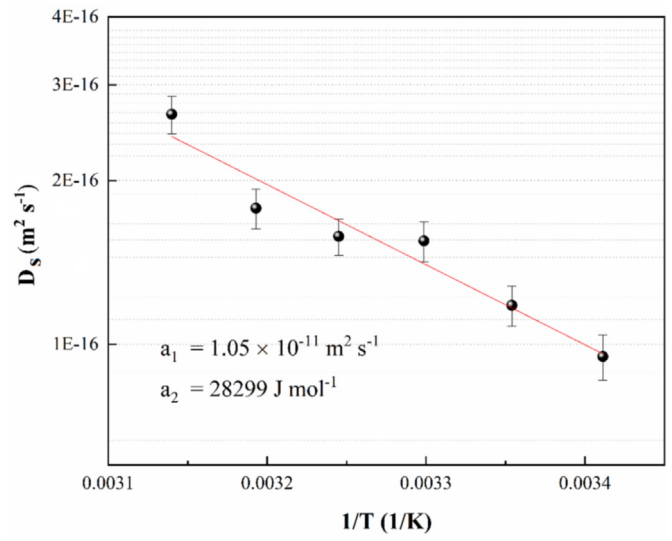

Fig. 7. The variation of intracrystalline diffusion against the inverse temperature. The experimentally measured data (Scatter) and the fitting curve (Line) (R-square: 0.9566).

(Desorption). Fig. 8(a–b) have shown the variation of cyclic uptake during the ad/desorption process. Based on the volume integration in the COMSOL, the calculated mass variation of the adsorbed water vapor matches well with the measured values shown in Fig. 8 (a) and (b), and the overall discrepancies are within a reasonable range of ±20% (Fig. 8(c)), which demonstrates a high fidelity model. In addition, the results from experiments indicated that the adsorption process is slower than the desorption process according to the time spent to the equilibrium state, and this can be explained by the increase in the intracrystalline diffusivity due to a higher surface temperature, which conforms to the Eqs. (4) and (10). With 0.25 mm (0.142 g) and 0.8 mm (0.463 g) of coatings, 0.25 mm of coating has a larger adsorption and desorption rate than the one with 0.8 mm. The major problem is that the thicker coating can lead to a larger thermal resistance to thermal diffusion, especially in the case of isosteric heat. For MOF-160(Al), it is noted that 70 °C can drive the desiccant regeneration [25], which is outperforming most of the conventional desiccants (zeolites, >90 °C [34]).

Considering the aspect ratio of **z**: **x** (0.025 cm: 4 cm and 0.08 cm: 4 cm), the observed cross-section was shown in Fig. 8(d). With the thickness of 0.025 cm and 0.08 cm, Fig. 8(e) and (g) demonstrated that a certain ratio of vapor was retained initially in the coating, even after a high-temperature regeneration process. In Fig. 8(f) and (h), the coatings of 0.025 cm and 0.08 cm can approach the saturated state at the end of each adsorption process, which is close to the maximum adsorption capacity shown in Fig. 5.

4.4.2. Parameter studies

Before the parameter studies, the surrounding conditions are to be provided. For consistency, it is assumed that surrounding air was maintained at 21 °C and 0.0118 kg m^{-3}, and the corresponding properties of the desiccant were listed in Table 2. The bottom temperature during the adsorption process was set at 20 °C to guarantee the isothermal adsorption, which reduces the adverse effect of the isosteric heat. The air velocity over the surface of the desiccant coating is neglected. To measure the sorption performance, the volumetric uptake, U_m, is determined as a function of time, which is evaluated as follows:

$$U_m = \overline{\omega_i}\rho_d(1-\varepsilon) \tag{19}$$

where $\overline{\omega_i}$ represents the average uptake [kg kg^{-1}] at the time of *i*.

1) Cycle time and diffusivity

In this study, the variation of U_m with time is calculated using the validated model. Given that the thickness of MOF coating is set at 0.25 mm, we investigate the effect of these factors on the sorption performance of MIL-160(Al).

Fig. (9) compares the temporal variation of volumetric uptake with the different time ratios of adsorption to desorption (t_{AD}: t_{DE}). It can be found that under each given cycle time, the optimization of the time ratio (t_{AD}: t_{DE}) can maximum the cyclic performance. As the cycle time extended (Fig.9 (a)–(c)), the adsorption process gradually approaches the equilibrium state after 1000s. Based on the vapor transport inside the desiccant layer, Eqs. (1) and (10) can demonstrate that the vapor transport is dominated by either intercrystalline (D_v) or intracrystalline (D_s) diffusivity. In this study, the characteristic time taken for the intercrystalline diffusivity ($\delta^2/D_v \sim 10^2 s$) is much less than that of the intracrystalline diffusivity ($d^2/D_s \sim 10^3 s$), which indicates that the intracrystalline diffusivity determines the time to the equilibrium state for the desiccant layer, conforming to the results in Fig. 9(c).

Apart from the time ratio and cycle time, Eq. (10) indicates that the crystal size and diffusivity can also affect the temporal variation in the volumetric uptake. Fig. 10 shows the variation of volumetric uptake with the same cycle time (1250s) and time ratio (t_{AD}: t_{DE} = 3:1, t_{AD} = 1000s) but different crystal sizes and diffusion. In Fig. 10(a), the increase in the crystal size can sharply reduce the net cyclic capacity, and extend the time to the equilibrium state for both the adsorption and desorption process. A similar phenomenon can also be found with the decrease in the diffusion in Fig. 10(b). The intracrystalline diffusivity is directly related to the transport of the adsorbed water and thus can affect the total sorption capacity. According to the analysis on the characteristic time for the intracrystalline diffusivity, the duration of the adsorption process should be close to the time scale as d^2/D_s, which means that for a given material the optimization should weigh the crystal size and diffusion to regulate the temporal variation of the volumetric uptake. A larger intracrystalline diffusivity will greatly reduce the time to the equilibrium state, from nearly1000s ($a_1 = 2 \times 10^{-11}$) to less than 250s ($a_1 = 5 \times 10^{-11}$).

In summary, the different combinations of these parameters can result in quite different shapes in the temporal variation of U_m. Here the intracrystalline diffusivity depends on the selection of the desiccant materials (the nature of desiccant), while crystal size can maximum the sorption performance from the structure level. In addition, the strategy for the optimization of cycle time and time ratio can make full use of the desiccant layers within the desired time (AD & DE). Assumed that the isosteric heat can be removed by the heat source from the bottom surface immediately, it enables a fast vapor concentration regulation (strong dynamics).

2) Porosity and characteristic length (thickness)

Considering the vapor transport theory, it is clear that the porous materials with high porosity can increase the possibility of collision between water vapor molecules and the materials, but leading to the decrease of the net cyclic capacity. The variation of the thickness, however, can improve the net cyclic capacity, if the isothermal conditions are well provided. Thus, for the desiccant layer with a given porosity, the reasonable thickness of the desiccant layer benefits the sorption performance. Given that the reasonable combinations of the parameters discussed above (t_{cycle} = 1250s, t_{AD}: t_{DE} = 4:1 and d = 1.5 μm) are applied, Fig. 11

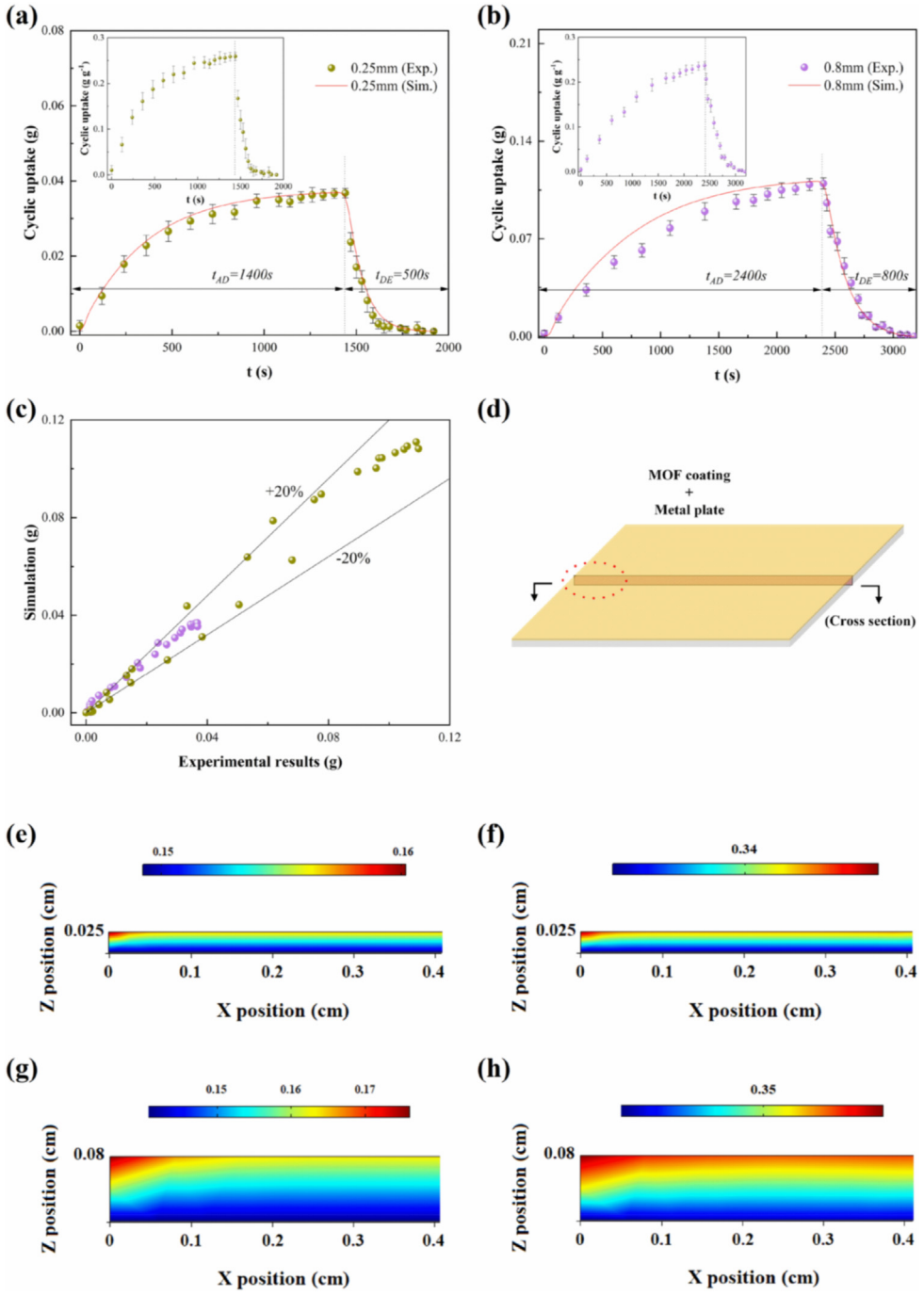

Fig. 8. The mass variation of the adsorbed water vapor on MIL-160(Al). (a–b) Validation with thickness δ = 0.25 mm and 0.8 mm; (c) Comparison between experimental results and simulation; (d) Observed cross section; (e) and (g) Initial adsorption state; (f) and (h) Final adsorption state.

shows the calculated total amount of the cyclic capacity ($= U_m * V = U_m * A * \delta$) with different porosity and thickness.

In Fig. 11(a), it can be found that the porosity has a certain effect on the sorption performance, leading to the increase of the net cyclic capacity as the porosity decreases. Though the higher stacking density is preferable, a much lower porosity may impede the vapor transport. Besides, Fig. 11(b) shows the variation in the cyclic capacity with different thicknesses. For a given porosity, the increase in the coating thickness can to some extent improve the sorption performance. Considering the thermal resistance and the release of isosteric heat, the correlation of the cyclic capacity to the coating thickness varies from linear to nonlinear.

3) Regeneration and surrounding vapor pressure

From the measurements of isotherms on MIL-160(Al), the temperature variation can lead to a change in water uptake, more specifically, the water uptake variation at different vapor pressure. It is preferable to consume a small amount of energy to drive the ad/desorption cycles because a high regeneration temperature requires more energy input. Here the sorption performance of MIL-160(Al) with different regeneration conditions (T_{reg} = 50 °C,

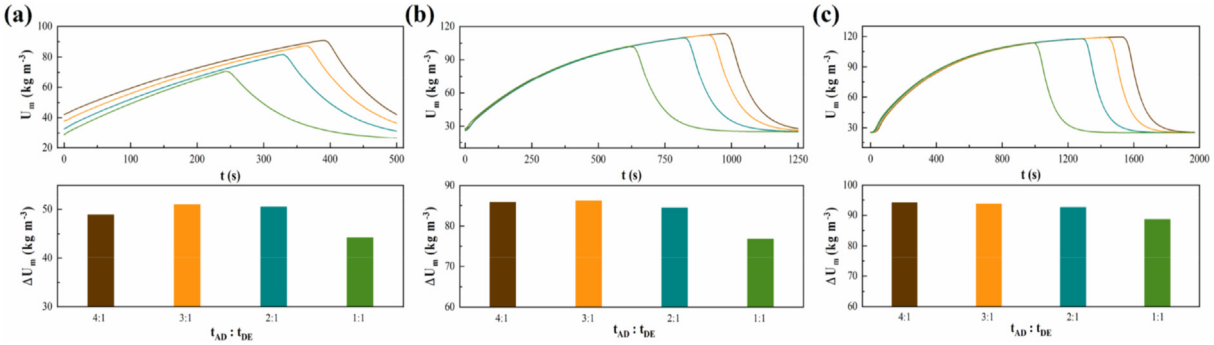

Fig. 9. The effect of time ratio at different cycle times on the variation of the volumetric uptake and the net cyclic capacity.

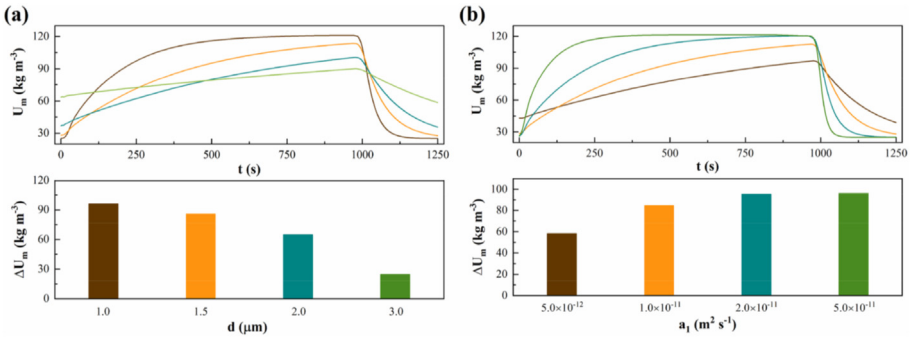

Fig. 10. The effect of crystal size and diffusion on the variation of the volumetric uptake and the net cyclic capacity.

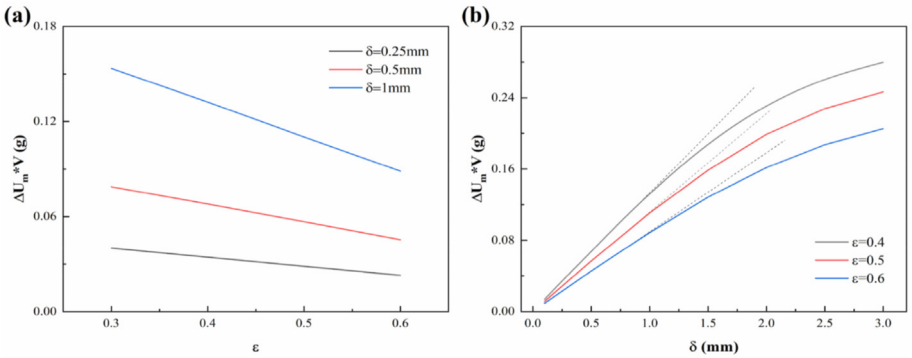

Fig. 11. Variation of the net cyclic capacity shown as a function of a) porosity and b) thickness.

70 °C, and 90 °C) has been simulated in the comparison with one commercial material zeolite 13X [28]. The given simulation conditions (t_{cycle} = 1250s, t_{AD}: t_{DE} = 4:1, δ = 0.25 mm and d = 1.5 μm) were provided (see Fig. 12).

Based on Eq. (18), the intracrystalline diffusivity changed as the temperature varied. During the adsorption process, the regeneration temperature can affect the amount of adsorbed vapor and then change the average ad/desorption rate. The increase in the regeneration temperature can achieve fast desorption, but the cycling uptake has been boosted limitedly, from 37 kg m^{-3}→ 86 kg m^{-3} (50°C→70 °C) to 86 kg m^{-3}→105 kg m^{-3} (70°C→ 90 °C). The bottom temperature of 70 °C during the desorption process is enough to regenerate the MIL-160(Al). In addition, the effect of the surrounding vapor pressure has also been investigated, which is shown as a function of the relative pressure of the surrounding air in Fig. 13. It can be found that the vapor pressure of the surrounding air has a limited effect on the net cyclic capacity in the high RH range (RH ≥ 50%), showing a slight decrease as RH increases. In addition to the investigation on the different surrounding vapor pressure, Fig. 14 has clearly shown the effect of different surrounding air temperatures on the variation of volumetric uptake. It indicates that MIL-160(Al) is sensitive to the surrounding air temperature under the same relative humidity condition compared with zeolite 13X, but both of them experience a little variation of volumetric uptake under the same vapor concentration conditions.

5. Conclusion

It is known that the adsorption-based system can improve the whole system's performance when regenerated by low-grade energy such as waste heat and solar energy. Currently, there are many numerical works reported to investigate the sorption performance

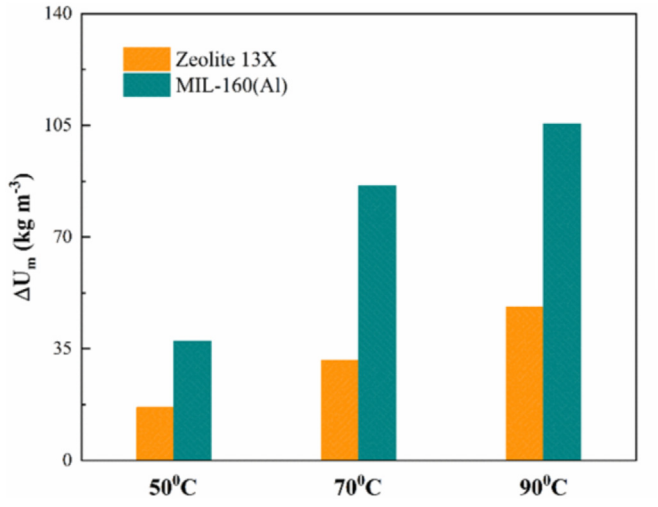

Fig. 12. The effect of regeneration temperature on the net cyclic capacity.

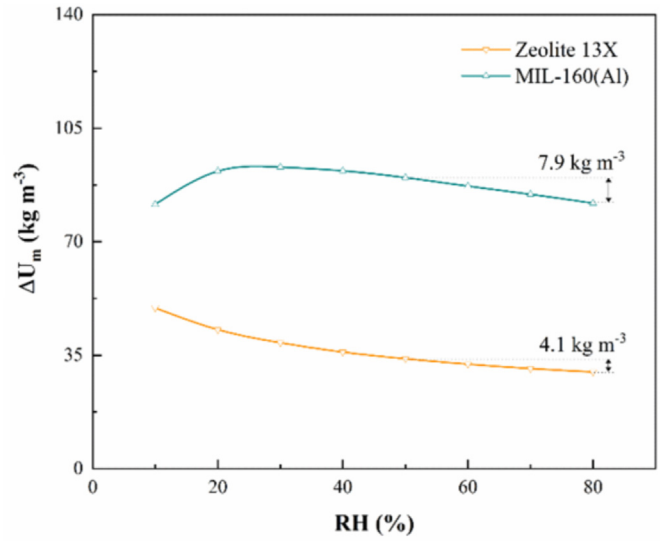

Fig. 13. The effect of the surrounding vapor pressure on the net cyclic capacity (T_{reg} = 70 °C).

simulations. In this study, MIL-160(Al) was successfully synthesized through the solvothermal method. The measured SEM characteristics of this MOF sample have shown its crystal structure illustrating the vapor diffusion between crystals. The isotherms of MIL-160(Al) indicated its ad/desorption processes under different vapor pressure and temperature conditions. Based on the Langmurian sorption isotherm, the measured water uptake featuring S-shaped curves matched well with the results from the theoretical model given as a function of temperature and vapor pressure. The calculated isosteric heat of MIL-160(Al) was consistent with the measured values reported in the other document, and the intracrystalline diffusivity can be obtained from the experiments, which explains a faster desorption rate than the adsorption one.

To observe the sorption dynamics of MIL-160(Al) samples, different thicknesses of the MOF layer were prepared and put on the climate chamber. The simulated results match well with the experiments, which demonstrate that we developed a fidelity mathematical model. Based on the mathematical modeling, some parametric studies about MIL-160(Al) were conducted and some conclusions can be obtained:

1) Under the given surrounding conditions, the time from the beginning to the equilibrium state is determined by the intracrystalline diffusivity, which affects the duration of a whole cycle. And the reasonable time ratio of the cycle can make full use of the desiccant coating. Besides, the optimization of the ad/desorption process can also be regulated by weighing the crystal size and the selected material.
2) Material properties such as porosity can affect the vapor transport and the stack density, but the sorption performance is limited as the porosity increases. As for the desiccant layer with a given porosity, the appropriate increase of the coating thickness can also improve the net cyclic capacity. Considering the release of isosteric heat, the increasing trend of the net cyclic capacity was obviously weakened as the thickness increases. Thus, after determining the length of a cycle time, the sorption performance is related to the coating thickness and its porosity. Intracrystalline diffusivity related to temperature variation can affect the ad/desorption rate, leading to an obvious change in sorption dynamics. The balance between the sorption performance and regeneration conditions pointed out that 70 °C is enough to regenerate the MIL-160(Al) coating while the thickness is around 0.025 cm.

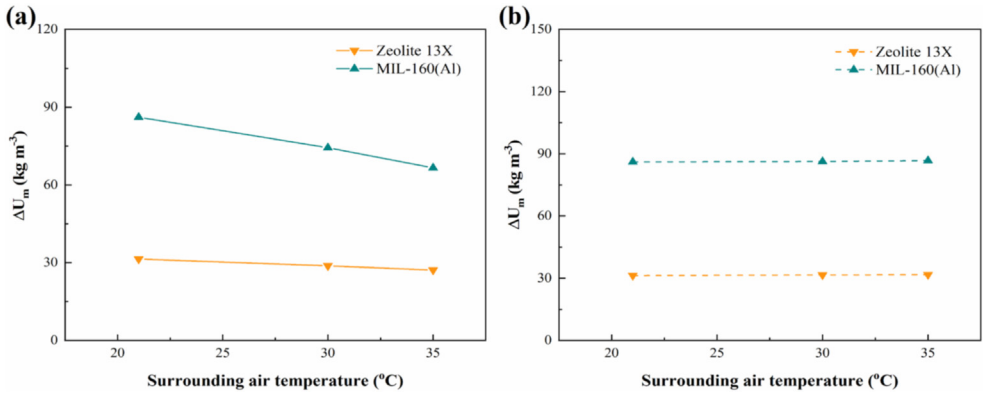

Fig. 14. The effect of different surrounding air temperatures on the net cyclic capacity (T_{reg} = 70 °C). a) RH = 65%; b) ρ_0 = 0.0118 kg m^{-3}.

of solid desiccant systems, but the performance of MIL-160(Al) on vapor transport was barely reported from experiments and

3) Compared with the commercial material (zeolite 13X), the balance between the sorption performance and regeneration

conditions pointed out that 70 °C is enough to regenerate the MIL-160(Al) coating of 0.25 mm. And the surrounding vapor pressure (i.e. RH) has a limited effect on the net cyclic capacity of MIL-160(Al) in the high RH range (RH $\geq$ 50%), while the increase of the surrounding air temperature may lead to the decline in the net cyclic capacity under the same RH condition.

Since there are many parameters that could play an important role in the operating performance of a solid desiccant system, computational analysis can provide the insights to design and optimize the MIL-160(Al) used solid desiccant systems. In this regard, green biomass-derived MIL-160(Al) outperforms some conventional materials (i.e. zeolites) and MOFs (i.e. Cr-based) in either sorption capacity, regeneration conditions or toxicity.

Declaration of competing interest

The authors declare that they have no known competing financial interests or personal relationships that could have appeared to influence the work reported in this paper.

Acknowledgments

The authors acknowledge the financial support from Bjarne Saxhof's Foundation and the Chinese Scholarship Council (No. 201806230288). We would like to thank S. Cui for the measured data of material properties of MIL-160(Al).

Nomenclature

c_{pm}	Specific heat of the desiccant [J $(kg \cdot K)^{-1}$]
c_{pv}	Specific heat of vapor phase [J $(kg \cdot K)^{-1}$]
c_{pw}	Specific heat of the adsorbed water vapor [J $(kg \cdot K)^{-1}$]
d	Equivalent diameter of the desiccant crystal [m]
$\overline{d}$	Intercrystalline pore diameter [m]
D_s	Intracrystalline diffusivity [m^2 s^{-1}]
D_v	Intercrystalline diffusivity [m^2 s^{-1}]
h_v	Heat transfer coefficient [W $(m^2 \cdot K)^{-1}$]
P	Vapor pressure [Pa]
P_0	Initial vapor pressure [Pa]
q_{ah}	Adsorption heat [kJ mol^{-1}]
R	Universal gas constant [J $(mol \cdot K)^{-1}$]
ΔQ	Adsorption characteristics energy [kJ kg^{-1}]
t	Time [s]
T	Temperature [K]
T_a	Chamber air temperature [K]
T_0	Initial temperature [K]
T_s	Bottom side temperature [K]
T_{wall}	Wall temperature [K]
u	Velocity [m s^{-1}]
U_m	Volumetric uptake [kg m^{-3}]
x, y, z	3D coordinate [m]

Greek symbols

α, β	Fitting parameters
ω	The amount of the adsorbed water vapor [kg kg^{-1}]
ω_{eq}	The equilibrium amount of the adsorbed water vapor [kg kg^{-1}]
$\overline{\omega_i}$	Average uptake [kg kg^{-1}]
σ	Stefan-Boltzmann constant [W $(m^{-2} \cdot K^{-4})$]
ρ	Concentration of vapor [kg m^{-3}]
ρ_d	Concentration of the adsorbed water vapor [kg m^{-3}]
ε	Emissivity
ε	Porosity
λ	Thermal conductivity [W $(m \cdot K)^{-1}$]

Credit author statement

Kan Zu: Investigation, Methodology, Writing – original draft, Menghao Qin: Conceptualization, Supervision, Writing – review & editing.

References

[1] Pérez-Lombard L, Ortiz J, Pout C. A review on buildings energy consumption information. Energy Build 2008;40:394–8.
[2] Zhao H, Magoulès F. A review on the prediction of building energy consumption. Renew Sustain Energy Rev 2012;16:3586–92.
[3] Chua KJ, Chou SK, Yang WM, Yan J. Achieving better energy-efficient air conditioning – a review of technologies and strategies. Appl Energy 2013;104:87–104.
[4] Benhadid-Dib S, Benzaoui A. Refrigerants and their environmental impact substitution of hydro chlorofluorocarbon HCFC and HFC hydro fluorocarbon. Search for an adequate refrigerant. Energy Procedia 2012;18:807–16.
[5] Wu Z, Qin M, Zhang M. Phase change humidity control material and its impact on building energy consumption. Energy Build 2018;174:254–61.
[6] Cui S, Qin M, Marandi A, Steggles V, Wang S, et al. Metal-Organic Frameworks as advanced moisture sorbents for energy-efficient high temperature cooling. Sci Rep 2018;8:15284.
[7] Sah RP, Choudhury B, Das RK. A review on adsorption cooling systems with silica gel and carbon as adsorbents. Renew Sustain Energy Rev 2015;45:123–34.
[8] Mohammed RH, Mesalhy O, Elsayed ML, Chow LC. Assessment of numerical models in the evaluation of adsorption cooling system performance. Int J Refrig 2019;99:166–75.
[9] Teo HWB, Chakraborty A, Kitagawa Y, Kayal S. Experimental study of isotherms and kinetics for adsorption of water on Aluminium Fumarate. Int J Heat Mass Tran 2017;114:621–7.
[10] Berezin GI, Kiselev AV. Adsorbate-adsorbate association on a homogenous surface of a nonspecific adsorbent. J Colloid Interface Sci 1972;38:227–33.
[11] Ugale VD, Pitale AD. A review on working pair used in adsorption cooling system. Int. J. Air-Conditioning Refrig. 2015;23:1530001.
[12] Henninger SK, Jeremias F, Kummer H, Janiak C. MOFs for use in adsorption heat pump processes. Eur J Inorg Chem 2012:2625–34. 2012.
[13] de Lange MF, Verouden KJFM, Vlugt TJH, Gascon J, Kapteijn F. Adsorption-driven heat pumps: the potential of metal–organic frameworks. Chem Rev 2015;115:12205–50.
[14] Feng X, Qin M, Cui S, et al. Metal-organic framework MIL-100 (Fe) as a novel moisture buffer material for energy-efficient indoor humidity control. Build Environ 2018;145:234–42.
[15] Seo YK, Yoon JW, Lee JS, Hwang YK, Jun CH, Chang JS, Wuttke S, Bazin P, Vimont A, Daturi M, Bourrelly S, Llewellyn PL, Horcajada P, Serre C, Ferey G. Energy-Efficient dehumidification over hierachically porous metal–organic frameworks as advanced water adsorbents. Adv Mater 2012;24:806–10.
[16] Xu F, Bian ZF, Ge TS, Dai YJ, Wang CH, Kawi S. Analysis on solar energy powered cooling system based on desiccant coated heat exchanger using metal-organic framework. Energy 2019;177:211–21.
[17] Bareschino P, Diglio G, Pepe F, Angrisani G, Roselli C, Sasso M. Numerical study of a MIL101 metal organic framework based desiccant cooling system for air conditioning applications. Appl Therm Eng 2017;124:641–51.
[18] Wang S, Lee JS, Wahiduzzaman M, Park J, Muschi M, Corcos CM, Tissot A, Cho KH, Marrot J, Shepard W, Maurin G, Chang JS, Serre C. A robust large-pore zirconium carboxylate metal–organic framework for energy-efficient water-sorption-driven refrigeration. Nat. Energy 2018;3:985–93.
[19] Lenzen D, Zhao J, Ernst SJ, Wahiduzzaman M, Inge AK, Frohlich D, Xu H, Bart HJ, Janiak C, Henninger S, Maurin G, Zou X, Stock N. A metal–organic framework for efficient water-based ultra-low-temperature-driven cooling. Nat Commun 2019;10:3025.
[20] Permyakova A, Skrylnyk O, Courbon E, Affram M, Wang S, Lee UH, Valekar AH, Nouar F, Mouchaham G, Devic T, 14 Weireld GD, Chang JS, Steunou N, Frère M, Serre C. Synthesis optimization, shaping, and heat reallocation evaluation of the hydrophilic metal–organic framework MIL-160(Al). ChemSusChem 2017;10:1419–26.
[21] Wahiduzzaman M, Lenzen D, Maurin G, Stock N, Wharmby MT. Rietveld refinement of MIL-160 and its structural flexibility upon H2O and N2 adsorption. Eur J Inorg Chem 2018:3626–32. 2018.
[22] Gordeeva LG, Solovyeva MV, Sapienza A, Aristov YI. Potable water extraction from the atmosphere: potential of MOFs. Renew Energy 2020;148:72–80.
[23] Qin M, Hou P, Wu Z, Wang J. Precise humidity control materials for autonomous regulation of indoor moisture. Build Environ 2020;169:106581.
[24] Cadiau A, Lee JS, Borges DD, Fabry P, Devic T, et al. Design of hydrophilic metal organic framework water adsorbents for heat reallocation. Adv Mater 2015;27:4775–80.
[25] Permyakova A, Skrylnyk O, Courbon E, Affram M, Wang SJ, et al. Synthesis optimization, shaping, and heat reallocation evaluation of the hydrophilic metal–organic framework MIL-160(Al). ChemSusChem 2017;10:1419–26.

[26] Wahiduzzaman M, Lenzen D, Maurin G, Stock N, Wharmby MT. Rietveld refinement of MIL-160 and its structural flexibility upon H_2O and N_2 adsorption. Eur J Inorg Chem 2019:3626–32.
[27] Cui S, Marandi A, Lebourleux G, Thimon M, Bourdon M. Heat properties of a hydrophilic carboxylate-based MOF for wateradsorption applications. Appl Therm Eng 2019;161:114135.
[28] Chan KC, Chao CYH, Sze-To GN, Hui KS. Performance predictions for a new zeolite 13X/CaCl2 composite adsorbent for adsorption cooling systems. Int J Heat Mass Tran 2012;55:3214–24.
[29] Leong KC, Liu Y. System performance of a combined heat and mass recovery adsorption cooling cycle: a parametric study. Int J Heat Mass Tran 2006;49:2703–11.
[30] Qin M, Belarbi R. Development of an analytical method for simultaneous heat and moisture transfer in building materials utilizing transfer function method. J Mater Civ Eng 2005;17(5):492–7. https://doi.org/10.1061/(ASCE)0899-1561(2005)17:5(492).
[31] Hsu CT, Cheng P, Wong KW. Modified Zehner-Schlunder models for stagnant thermal conductivity of porous media. Int J Heat Mass Tran 1994;37:2751–9.
[32] Sakoda A, Suzuki M. Fundamental study on solar powered adsorption cooling system. J Chem Eng Jpn 1984;17:52–7.
[33] Elsayed E, Dadah RAL, Mahmoud S, Anderson P, Elsayed A. Adsorption cooling system employing novel MIL-101(Cr)/$CaCl_2$ composites: numerical study. Int J Refrig 2019;107:246–61.
[34] Chang K, Wang H, Chung T. Effect of regeneration conditions on the adsorption dehumidification process in packed silica gel beds. Appl Therm Eng 2004;24:735–42.